Review Article

Cardiac MR imaging: current status and future direction

Maythem Saeed[1], Tu Anh Van[2], Roland Krug[1], Steven W. Hetts[1], Mark W. Wilson[1]

[1]Department of Radiology and Biomedical Imaging, School of Medicine, University of California San Francisco, San Francisco, CA, USA; [2]Zentralinstitut für Medizintechnik, Technical University of Munich, Munich, Germany

Contributions: (I) Conception and design: M Saeed; (II) Financial support: NA; (III) Administrative support: Loi Do; (IV) Provision of study materials or patients: M Saeed; (V) Collection and assembly of data: M Saeed, TA Van, R Krug; (VI) Data analysis and interpretation: M Saeed, TA Van; (VII) Manuscript writing: All authors; (VIII) Final approval of manuscript: All authors.

Correspondence to: Maythem Saeed. Professor of Radiology and Biomedical Imaging, Department of Radiology and Biomedical Imaging, University of California San Francisco, 185 Berry Street, Suite 350, Campus Box 0946, San Francisco, CA 94107-5705, USA. Email: Maythem.Saeed@ucsf.edu.

Abstract: Coronary artery disease is currently a worldwide epidemic with increasing impact on healthcare systems. Magnetic resonance imaging (MRI) sequences give complementary information on LV function, regional perfusion, angiogenesis, myocardial viability and orientations of myocytes. T2-weighted short-tau inversion recovery (T2-STIR), fat suppression and black blood sequences have been frequently used for detecting edematous area at risk (AAR) of infarction. T2 mapping, however, indicated that the edematous reaction in acute myocardial infarct (AMI) is not stable and warranted the use of edematous area in evaluating therapies. On the other hand, cine MRI demonstrated reproducible data on LV function in healthy volunteers and LV remodeling in patients. Noninvasive first pass perfusion, using exogenous tracer (gadolinium-based contrast media) and arterial spin labeling MRI, using endogenous tracer (water), are sensitive and useful techniques for evaluating myocardial perfusion and angiogenesis. Recently, new strategies have been developed to quantify myocardial viability using T1-mapping and equilibrium contrast enhanced MR techniques because existing delayed contrast enhancement MRI (DE-MRI) sequences are limited in detecting patchy microinfarct and diffuse fibrosis. These new techniques were successfully used for characterizing diffuse myocardial fibrosis associated with myocarditis, amyloidosis, sarcoidosis heart failure, aortic hypertrophic cardiomyopathy, congenital heart disease, restrictive cardiomyopathy, arrhythmogenic right ventricular dysplasia and hypertension). Diffusion MRI provides information regarding microscopic tissue structure, while diffusion tensor imaging (DTI) helps to characterize the myocardium and monitor the process of LV remodeling after AMI. Novel trends in hybrid imaging, such as cardiac positron emission tomography (PET)/MRI and optical imaging/MRI, are recently under intensive investigation. With the promise of higher spatial-temporal resolution and 3D coverage in the near future, cardiac MRI will be an indispensible tool in the diagnosis of cardiac diseases, coronary intervention and myocardial therapeutic delivery.

Keywords: Myocardial viability; magnetic resonance imaging (MRI); coronary artery disease

Submitted May 28, 2015. Accepted for publication Jun 17, 2015.
doi: 10.3978/j.issn.2223-3652.2015.06.07
View this article at: http://dx.doi.org/10.3978/j.issn.2223-3652.2015.06.07

Coronary artery disease still is the main cause of death worldwide in spite of recent improvements in therapeutic and interventional methods. With the introduction of revascularization therapy, using coronary artery bypass grafting and percutaneous coronary intervention (PCI), the need for identifying viable myocardium has arisen. Furthermore, by preoperatively assessing the transmural size of the infarct, the functional recovery of dysfunctional segments after revascularization therapy in patients with chronic LV dysfunction can be predicted (1-3).

A number of indirect techniques have been introduced to assess myocardial viability. These techniques are echocardiography (for assessing recovery of contractile function), fluoro-2-deoxygluclose (FDG) positron emission

© Cardiovascular Diagnosis and Therapy. All rights reserved.

tomography (PET) (for assessing glucose metabolism) and ^{201}Tl single-photon emission computed tomography (SPECT) in patients with ischemic heart disease. Unlike echocardiography, magnetic resonance imaging (MRI) does not present the limitations of the acoustic window. MRI also offers more spatial and temporal resolution than nuclear medicine modalities and better tissue characterization. In addition, MRI does not use ionizing radiation, which is another advantage in respect to other imaging modalities such as computed tomography (CT) or nuclear medicine (4). MR images are acquired with a high contrast between blood pool and myocardium using a steady state free precession (SSFP) sequence. Similar to echocardiography, cine MRI allows dynamic imaging of cardiac wall motion, but with superior endocardial border definition, facilitating more accurate wall motion assessment. Left ventricular function and mass, measured with cine MRI, are used in clinical practice as an endpoint in clinical trials (5,6). End-diastolic wall thickness is easy to measure; however, this indicator does not measure the size of myocardial infarct (MI).

Another method for detecting myocardial viability and critical coronary stenosis is perfusion MRI. With this technique a bolus of contrast media is used to visualize the delay in perfusion in ischemic myocardium compared to healthy myocardium. Perfusion of ischemic myocardium can be assessed quantitatively by calculating perfusion indices (curve upslope, maximum signal intensity and time to the peak). However, clinical studies indicated that MI size is a stronger predictor of future events than LV functional or perfusion parameters, where significant areas of stunning and/or hibernating may be present (7-9).

Unlike echocardiography, PET and SPECT, MRI has the unique ability to provide quantitative information on cardiac function, perfusion and viability. Delayed enhancement MRI (DE-MRI) provides high contrast between viable and nonviable myocardium, thus it has been frequently used for detecting and measuring MI size. Furthermore, discrimination between viable and infarcted myocardium allows patients to avoid the risks associated with revascularization therapy when they are unlikely to benefit. MRI examination for evaluating suspected coronary artery disease consists of T2-weighted imaging for area at risk (AAR) demonstration and DE-MRI for infarct visualization. A recent study using T2 mapping, however, indicated that edematous reaction during the first week after ischemia/reperfusion is not stable and warranted the use of edema extent in evaluating therapies (10). Inversion-recovery prepared T1-weighted gradient-echo (GRE) sequence after intravenous administration of a gadolinium-chelate demonstrates MI, microvascular obstruction (MVO) zone, patchy microinfarct and peri-infarct zone (incomplete infarct at the infarct border). Evidence suggests that the likely mechanism is different volumes of distribution of gadolinium-based MR contrast media in viable and infarcted myocardium (11). It should be noted that an increased volume of distribution occurs in both acute and chronic (scar) MI, as there is an increase in the interstitial space. In the former, the loss of sarcomere membrane integrity increases the potential interstitial volume, whereas in the latter, the presence of fibrotic tissue increases the interstitial space. Additionally, dynamic first pass perfusion and cine SSFP sequences are used for detection of perfusion deficits and LV remodeling. The main disadvantages of the current cardiac MRI sequences are breath-holds, the exam time, contrast media reaction and relatively high cost. New real-time MRI sequences eliminated part of these disadvantages.

Cardiac MRI

Cardiac MRI is a noninvasive, tomographic, nonionizing technique, thus it has been clinically used for assessing expansion of infarcted segments, late wall thinning of infarcted regions, LV volumes, distortion of LV shape and compensatory hypertrophy of non-infarcted myocardium (12). At UCSF, MRI is used for ischemic, non-ischemic heart diseases, hypertrophic cardiomyopathy as well as heart failure and congenital heart disease (13-16).

MRI pulse sequences are software programs that control the magnitude and timing of the radiofrequency (RF) pulses emitted by the RF transmitter, switching of the magnetic field gradient and data acquisition. The major components of a pulse sequence are the engines and modifiers. The engines include fast spin-echo (FSE), GRE, SSFP, echo-planar imaging (EPI), and single-shot versus segmented modes, while the modifiers include fat suppression (used to null the fat), inversion recovery pulse (used to null the blood and viable myocardium on DE-MRI, saturation-recover preparatory pulses (used with perfusion weighted imaging and cardiac tagging), Phase-contrast imaging with velocity-encoded imaging (for measurement of vascular blood flow, regurgitate fraction and strain) and parallel imaging (applicable to most forms of cardiac imaging). Parallel imaging is a robust method for accelerating the acquisition of MRI data, and has made possible many new applications, such as cardiac MR imaging. Parallel imaging works by acquiring a reduced amount of k-space data with an array of receiver coils. These

© Cardiovascular Diagnosis and Therapy. All rights reserved.

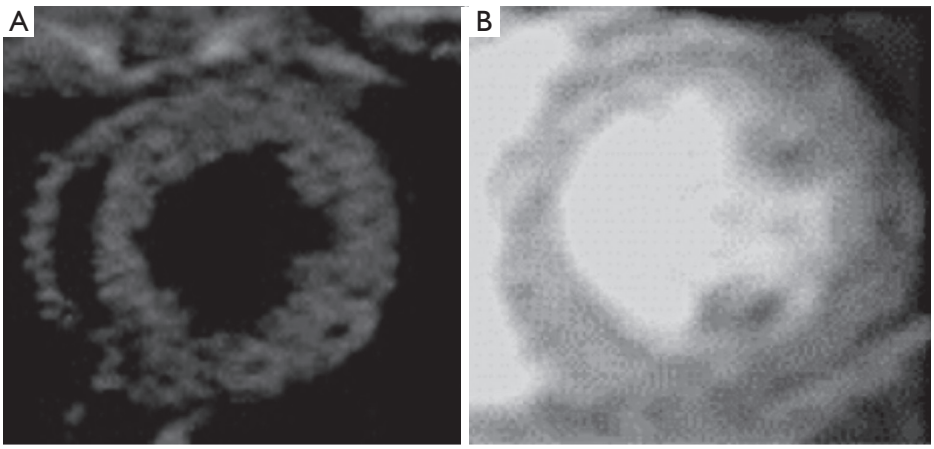

Figure 1 Black blood (spin echo, A) and bright blood (gradient echo, B) MRI images of the heart. MRI, magnetic resonance imaging.

undersampled data can be acquired more quickly, but the undersampling leads to aliased images. One of several parallel imaging algorithms can then be used to reconstruct artifact-free images from either the aliased images (SENSE-type reconstruction) or from the undersampled data (GRAPPA-type reconstruction). The advantages of parallel imaging in a clinical setting include faster image acquisition, which can be used, for instance, to shorten breath-hold times resulting in fewer motion-corrupted examinations. Several current applications of parallel imaging are presented and recent advancements and promising research in parallel imaging are well described by Heidemann *et al.* (17).

Bright blood imaging

In general, cardiac MRI sequences can be classified into either black-blood (spin-echo-based acquisitions) or bright-blood (GRE-based acquisition) sequences (*Figure 1*). Bright blood imaging sequences include GRE and SSFP. GRE sequences are also named spoiled gradient recall (SPGR), turbo FLASH, turbo field echo and fast-field echo (FFE) depending on the manufacturer of the scanner. The SSFP is the sequence of choice at 1.5T because of its high signal-to-noise ratio (SNR), which relies on a steady state of magnetization between the longitudinal and transverse magnetizations (T2/T1 ratio). This imaging sequence produces information on blood flow and cardiac function and has a spatial resolution of approximately 1.5×1.8 mm^2 and a temporal resolution of 50 ms. The signal in this sequence depends on steady-state T1 signal of blood and myocardium. Bright blood imaging describes the high signal intensity of fast-flowing blood and is typically used to evaluate global and segmental LV function. It has been used for measurements of LV mass, myocardial perfusion, blood flow and coronary anatomy. Investigators recommended cine SSFP sequence as an alternative to conventional echocardiograph.

Dark blood imaging

Dark blood imaging sequences refers to the low-signal-intensity appearance of fast-flowing blood and is mainly used to delineate LV chambers. Spin-echo (SE) sequences have been used for dark blood imaging and have relatively little artifact from metal (stents or other devices), but longer acquisition times compared with GRE. FSE dark blood T2-weighted sequences are used (double inversion-recovery, triple inversion-recovery, or short-tau inversion recovery (STIR) in the ventricular short axis. Unlike, conventional SE sequence, FSE and turbo spin-echo (TSE) techniques have lower SNR, but are faster than SE, which minimizes the effects of respiratory and cardiac motion. A potential source of artifact is bright slow-flowing blood adjacent to dysfunctional LV segment (*Figure 2*). It has been accepted that in acute myocardial infarct (AMI) the hyperintense territory on T2-STIR sequences reflects myocardium at risk (18). T2-mapping sequences have been used for quantitatively assessing myocardial edema (T2 relaxation time) and not qualitatively (arbitrary signal intensity) like T2-STIR sequences (19).

Dynamic first-pass perfusion imaging

Myocardial perfusion gives new insight into major and minor coronary artery disease. It can also be used as alternative

© Cardiovascular Diagnosis and Therapy. All rights reserved.

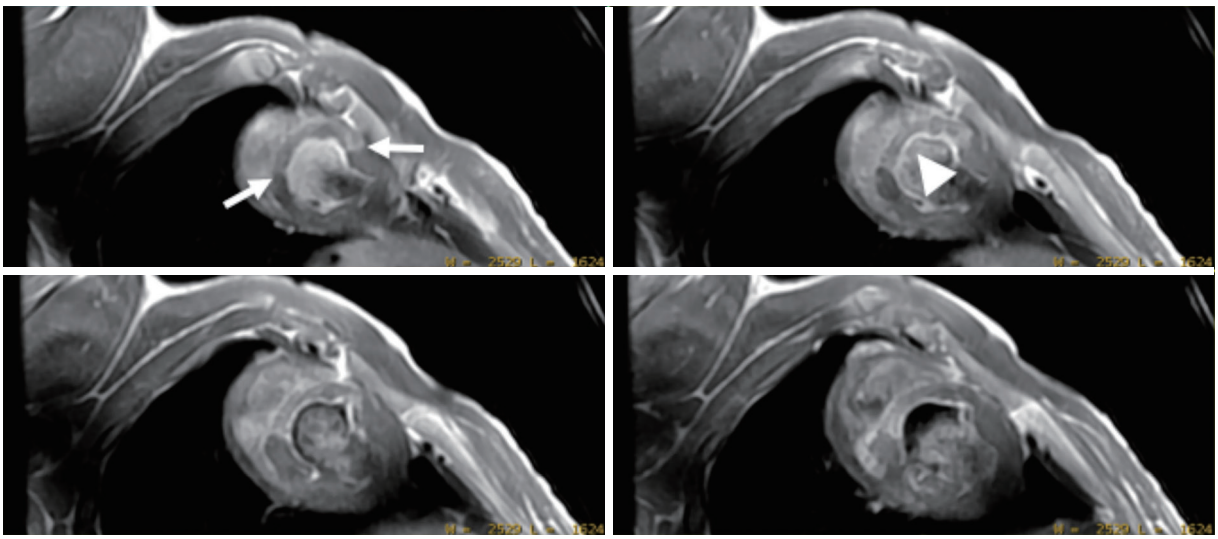

Figure 2 T2-weighted FSE images acquired on 3T scanner showing area at risk (edematous) at 3 days after AMI (arrows) and slow-flowing blood in the LA chamber (arrowhead). FSE, fast spin-echo; AMI, acute myocardial infarct.

surrogate endpoints in studies evaluating revascularization therapy and new therapeutic treatments, such as genes and stem cells. CT, ultrasound, PET and SPECT sequences are designed to obtain kinetic parameters that describe myocardial perfusion and microvascular permeability. Myocardial first pass perfusion sequences are T1-weighted GRE sequences, with a high temporal resolution acquired as gadolinium is being injected. With these sequences it is possible to monitor the contrast as it disseminates throughout the myocardium. Arterial spin-labeling MRI is also a sensitive and useful technique for evaluating myocardial perfusion and angiogenesis. Arterial spin labeling uses flow sensitive alternating inversion recovery MRI technique (20,21) with multiple inversion times and echo planar imaging readout and endogenous tracer (water). The arterial spin labeling technique allows the spin population in arterial water to be magnetically labeled by inversion pulse and used as an endogenous diffusible tracer (21-23). Unlike first-pass perfusion imaging, arterial spin labeling imaging technique has limited use in myocardial perfusion, because of confounding effects of cardiac motion and the relative modest signal changes achievable with spin labeling (24,25).

Unlike arterial spin labeling technique, first pass MRI perfusion uses exogenous tracers (gadolinium-based intravascular and extracellular MR contrast media). Fast perfusion images provide (I) strong T1 contrast; (II) large coverage of myocardial segments; and (III) adequate spatial resolution. Balanced SSFP, GRE and gradient echo-planar (GRE-EPI) are the fastest sequences for perfusion (26).

In multicenter trials, first-pass MRI perfusion demonstrated higher accuracy than SPECT in detecting ischemic myocardium (27). Perfusion sequences are typically more effective at 3T than 1.5T. The 109% higher SNR at 3T (28) can be used to improve spatial or temporal resolution. Peak enhancement is also better at 3T than 1.5T (29). The higher spatial resolutions achieved at 3T may result in decreased size and intensity of the dark rim artifact (Gibbs artifact) at the interface of the LV chamber and myocardium (30), a finding that often is confused with pathologic subendocardial ischemia and is believed to be secondary to low spatial resolution, susceptibility artifact or motion. At 3T, the diagnostic accuracy of myocardial perfusion deficit in coronary artery stenosis is 86% higher than at 1.5T, with good correlation with microspheres (31). *Figure 3* shows the correspondence between the perfusion deficits on first pass perfusion MRI, wall thinning and dysfunction in the infarcted wall on cine MRI and compensatory hypertrophy in remote myocardium on histochemical triphenyltetrazolium chloride (TTC) stain.

Delayed contrast enhanced MRI

Detection of myocardial viability is an important issue that needs to be addressed when patients with dysfunctional myocardium are considered for coronary revascularization. Viable myocardium can be detected with nuclear

© Cardiovascular Diagnosis and Therapy. All rights reserved.

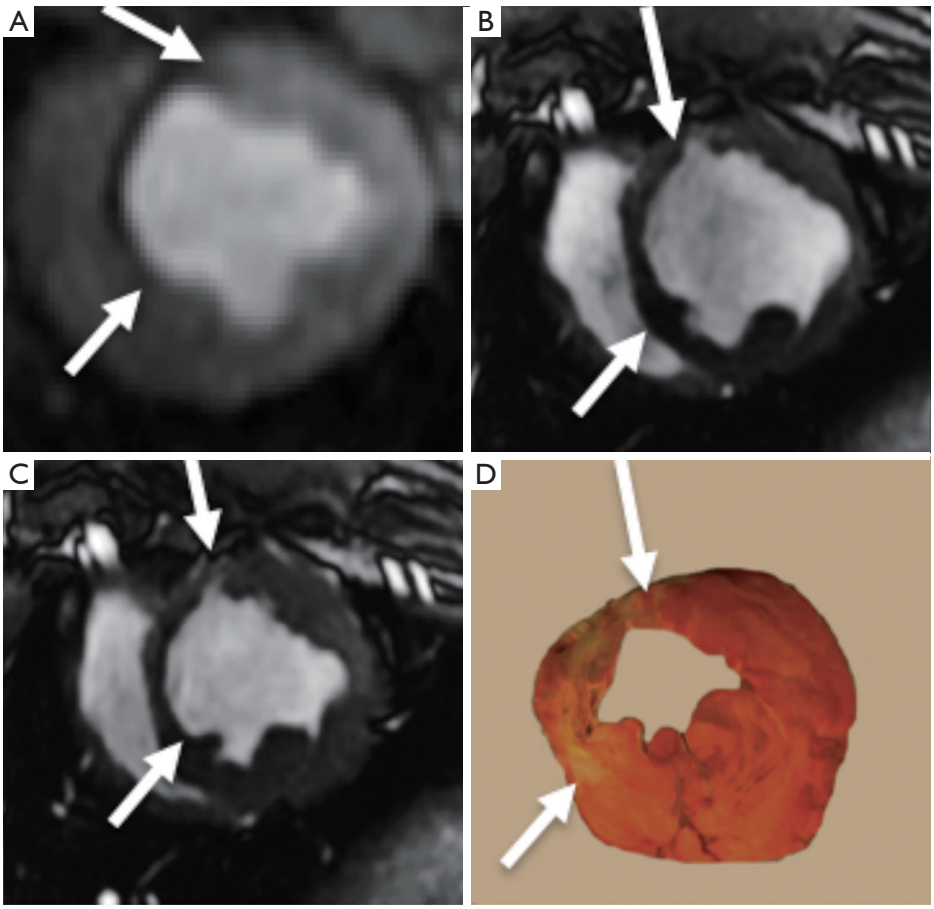

Figure 3 First pass perfusion (A), cine MR images of diastole (B) and systole (C) and stained LV section (triphenyltetrazolium chloride, TTC, D) show perfusion deficits (arrows, A), lack of wall thickening at systole (arrows, B,C), wall thinning at the site of infarction (arrows, D) and compensatory hypertrophy, respectively, at 5 weeks after infarction. TTC, triphenyltetrazolium chloride.

techniques (SPECT, PET), low dose dobutamine stress echocardiography and MRI. On MRI, detection of viable myocardium can be accomplished on T1 mapping, DE-MRI, dobutamine stress and stress/rest perfusion imaging.

T1-weighted 2D/3D GRE sequences with an inversion-recovery pulse were used for assessing myocardial viability (32). The inversion pulse is intended to cancel the signal of viable myocardium. New scanners often have a "look-locker (LL)" sequence that provides precise inversion time that nulls myocardial signal intensity at each time point post contrast injection. In infarcted myocardium, the inversion time (200 and 300 ms at 1.5T scanners and slightly higher at 3T) must be adjusted based on the imaging time after contrast media injection due to the clearance of gadolinium from the blood. DE-MRI is usually performed 10-15 min after injecting gadolinium-based MR contrast media. Because of the longer T1 of viable myocardium, the inversion time on 1.5T is shorter (260±30 ms) than 3T (330±48 ms). Several studies have demonstrated SNR and contrast-to-noise ratios (CNR) of up to 3.9 and 3.3 times higher at 3T than 1.5T, respectively (33,34) (*Figure 4*).

The sensitivity of DE-MRI for detection of AMI and scar is relatively high (99% and 94%, respectively) compared with SPECT (35,36). DE-MRI has the potential to demonstrate MI as small as 1 cm^3, which is substantially less than other imaging modalities (26,37-41). Some investigators also suggested that hyperenhanced myocardium on DE-MRI is a reliable parameter to predict true MI size. Early MRI studies in our lab, however, demonstrated that the hyper-enhanced region does not optimally delineate MI (11,42,43), because DE-MRI overestimates AMI by including the edematous border surrounding the infarct (peri-infarct zone). Since the

© Cardiovascular Diagnosis and Therapy. All rights reserved.

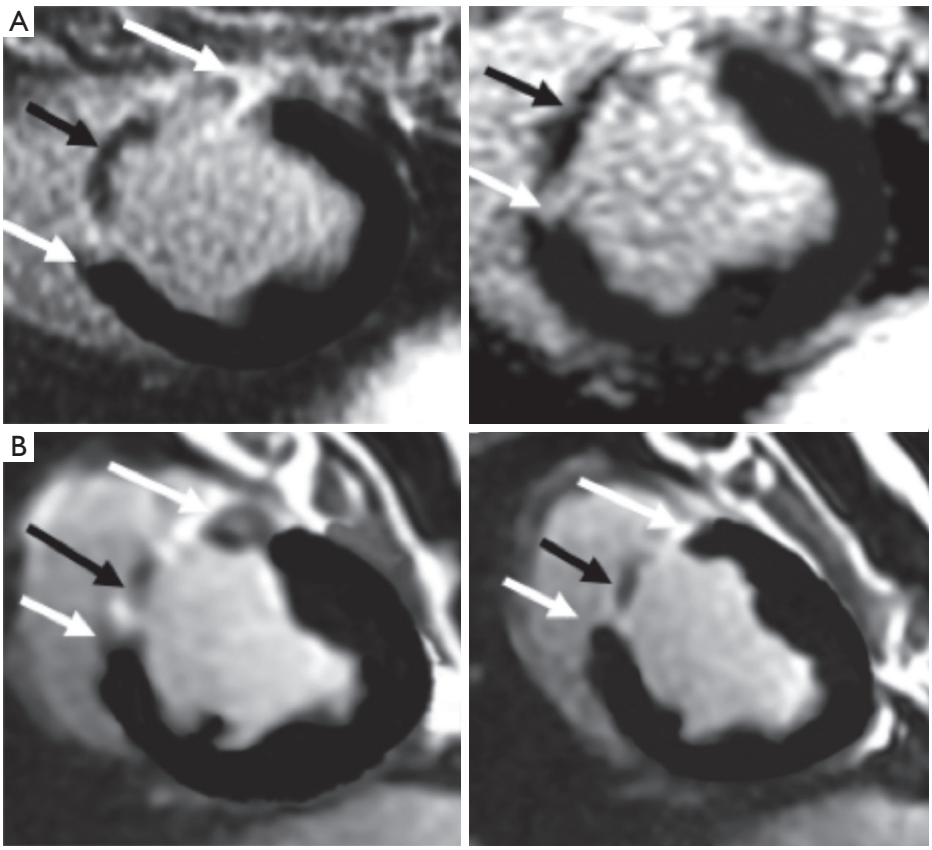

Figure 4 Multi-slice DE-MR images acquired on 1.5T (A) and 3T (B) scanners. Both field strength scanners revealed transmural AMI (white arrows) with microvascular obstruction in the core (black arrows). AMI, acute myocardial infarct.

extent of peri-infarct zone is time dependent, investigators considered it the target of gene and stem cell therapies. Others investigators consider it a source of arrhythmia and poor prognosis (44,45).

The principle of differential AMI on DE-MRI is that the cellular membrane is ruptured and an extracellular contrast media diffuses passively into the intracellular space resulting in increased signal intensity. In chronic myocardial infarctions, scar tissue mainly contains collagenous material; thus, there is an absence of the viable myocardium with increased extracellular space that results in increased contrast concentration and enhancement on DE-MRI (*Figures 5*,*6*). The detection of diffuse myocardial fibrosis is limited on DE-MRI, therefore investigators used myocardial T1 relaxivity for assessing the degree of fibrosis. This technique involves the estimation of the distribution volume of gadolinium in the myocardium based on T1 relaxivity of myocardium relative to that of the blood pool over time. Diffuse myocardial fibrosis has been identified in cases of heart failure, dilated cardiomyopathy and congenital heart disease.

DE-MRI identifies AMI/chronic MI, peri-infarct zone, as well as MVO with high spatial resolution independently from LV function. The transmural extent of hyperenhancement on DE-MRI has been used to predict functional recovery after revascularization in AMI. DE-MRI differentiates non-viable myocardium on the bases of contrast media distribution in infarcted and fibrotic tissues (*Figures 5*-7). Wu *et al*. (46) studied 122 patients with STEMI following acute percutaneous revascularization using DE-MRI. The investigators found that AMI size correlated linearly with the initial end systolic volume index, end-diastolic volume index and ejection fraction. Furthermore, Roes *et al*. (47) found that the size of hyperenhanced infarct on DE-MRI is superior to LVEF and LV volumes for predicting long-term mortality in patients. Masci *et al*. (48) have demonstrated that the size of hyperenhanced infarct on DE-MRI determines the pattern of infarct healing and regional and

© Cardiovascular Diagnosis and Therapy. All rights reserved.

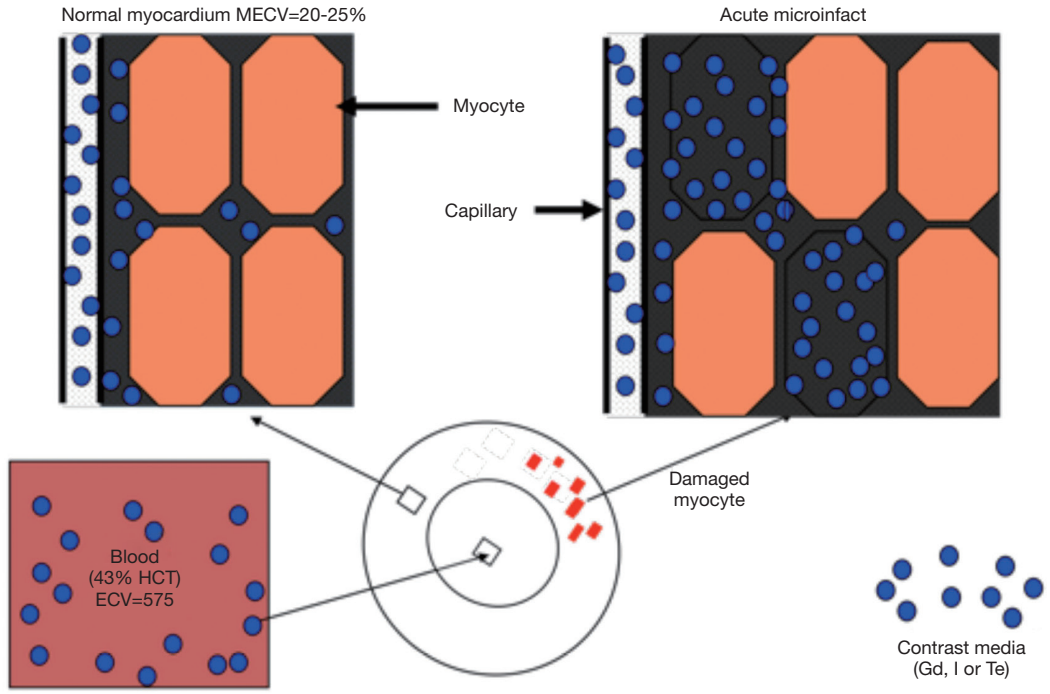

Figure 5 The three fluid compartments in healthy myocardium, namely intravascular (~10% of tissue volume), interstitial (~15%) and intracellular (~75%) compartments.

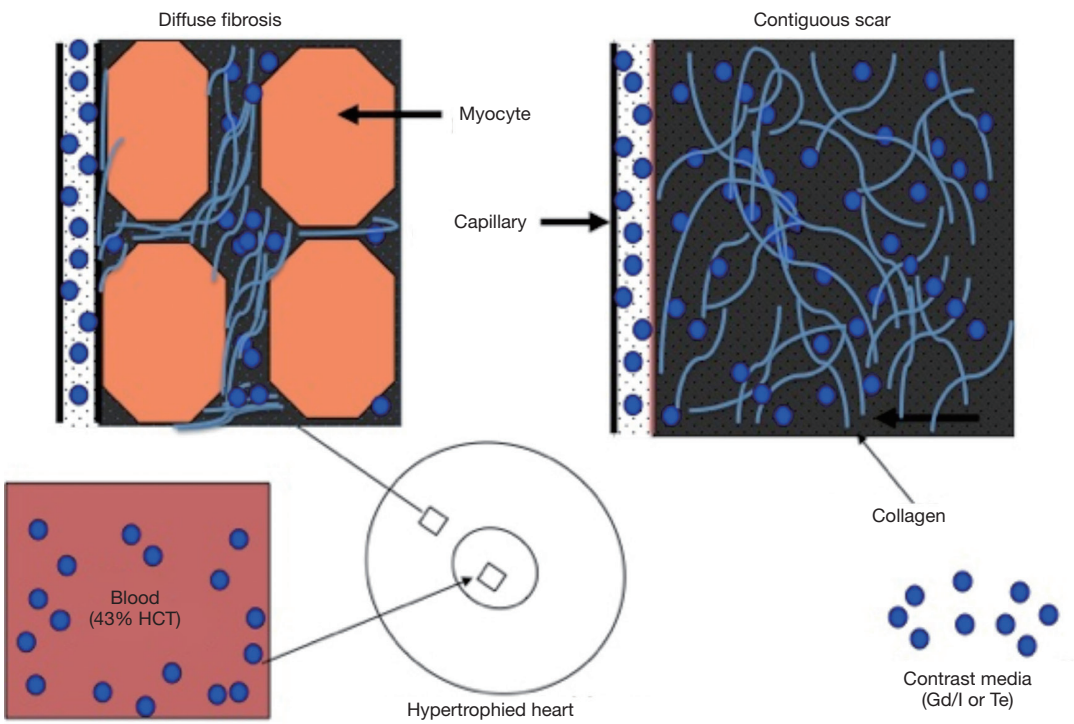

Figure 6 Schematic presentation of diffuse myocardial fibrosis in non-ischemic heart diseases (A) and contiguous chronic infarct (B) in ischemic heart disease.

© Cardiovascular Diagnosis and Therapy. All rights reserved.

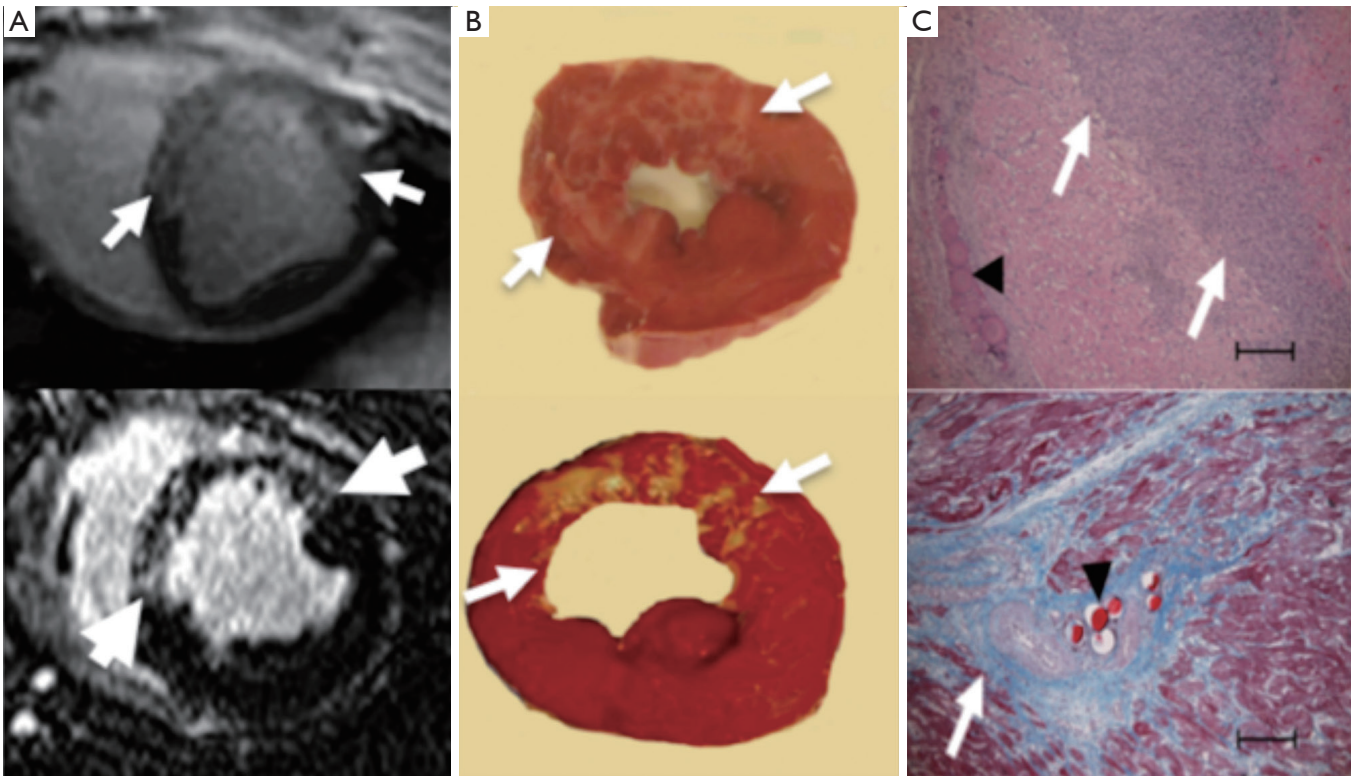

Figure 7 DE-MRI acquired on 1.5T scanner (A), histochemical triphenyltetrazolium chloride (TTC) stain (B) and histopathological stains (A) show patchy microinfarct (arrows) 3 days (top row) and 5 weeks (bottom row) after delivering a 32 mm^3 volume of 40-120 μm diameter microemboli in the LAD coronary artery in a swine model. Representative histopathology sections stained with hematoxylin and eosin for AMI (top C) and Masson trichrome (bottom C) stains reveal scar infarct (arrow) and microemboli (arrowhead) obstructing modified, thick wall and small lumen) blood vessels (scale =100 μm).

global LV remodeling. Currently, DE-MRI is recognized as the standard of reference for assessment of myocardial viability and the size and pattern of hyperenhanced infarct provides important prognostic information on ischemic and nonischemic cardiomyopathy (49).

Coronary revascularization for treating AMI is associated with MVO in the core and peri-infarct zone at the border. Ahmed *et al*. observed MVO zone in 20-50% of the patients after revascularization of AMI (50). MVO zones can be detected on MRI using three different strategies: first pass perfusion, early enhancement and delayed enhancement (8,51). The last two methods are more specific, because the first method shows the perfusion deficit in infarct with and without MVO zones. Imaging early (1-2 min) after gadolinium-based MR contrast media administration provides valuable information on MVO zone. The dark appearance of MVO zones on T1-weighted imaging is related to lack of delivery of MR contrast media to the infarct core. MVO zones subside on day 9 after infarction. In an experimental study, it has been demonstrated that hemorrhage occurs within MVO zones (52). Myocardial hemorrhage can be detected on T2 and T2* sequences. On T2 sequences it is identified as a hypointense area within the hyperintense edematous AAR. On T2* sequence the size of the hemorrhagic zone is smaller than MVO zone and is identified as a hypointense area (52). Multiple MR studies have shown that patients with large MVO zone have poor prognosis (51,53). Wu *et al*. found that the presence of MVO zone in AMI is a marker of poor prognosis (54).

We were the first to demonstrate the peri-infarct zone on DE-MRI in experimental animals (55). The major part of differentially enhanced myocardium on DE-MRI represents MI and the other small portion represent peri-infarct zone (45). Investigators found strong correlation between the extent of peri-infarct zone and ventricular arrhythmias and sudden death (44,45). Both MVO and

© Cardiovascular Diagnosis and Therapy. All rights reserved.

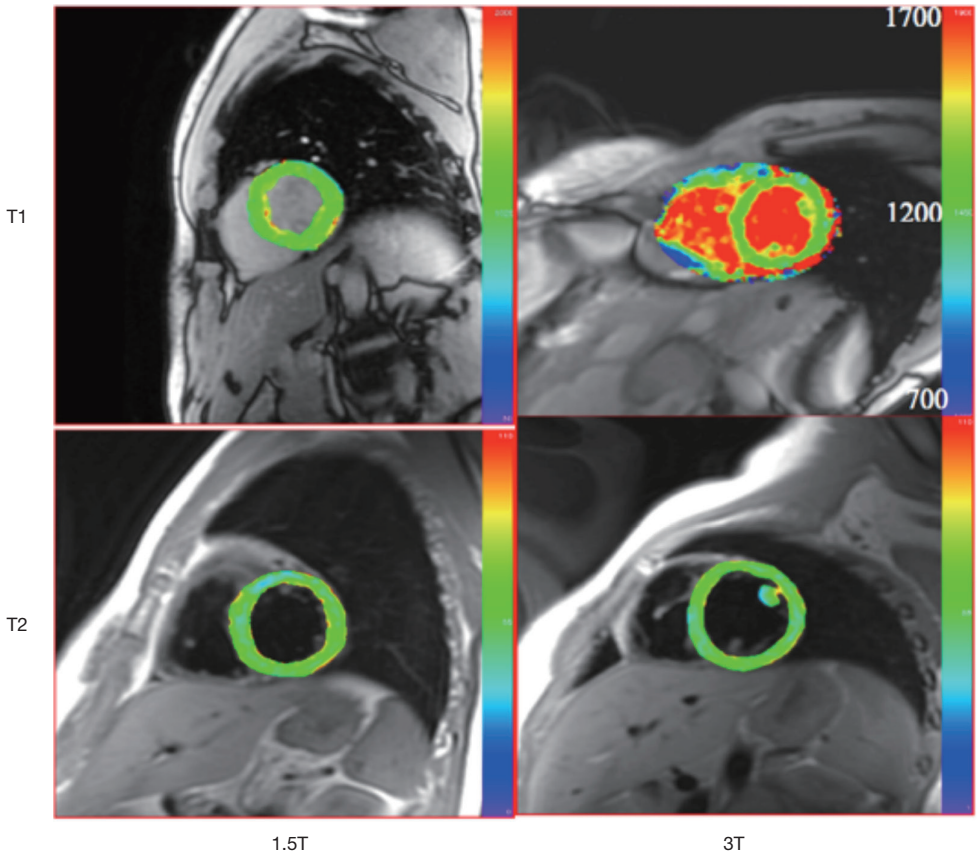

Figure 8 T1 and T2 maps of normal volunteer acquired at 1.5T and 3T field strengths. These techniques are useful in detecting focal and diffuse acute and scar infarct.

peri-infarct zones are visible and can be monitored on DE-MRI. In an electrophysiological study of 40 patients before implantation of pacemakers or implantable automatic defibrillators, the size of the peri-infarct zone on DE-MRI predicted ventricular tachycardia (56). Additionally, DE-MRI has the potential of measuring infarct resorption in animal models (57,58) and humans (59-61).

T1 mapping

T1 and T2 relaxation times with and without MR contrast media can be used for mapping myocardium (*Figure 8*) (19,62-64). LL, modified Look-Locker inversion-recovery (MOLLI) and shortened modified Look-Locker inversion-recovery (ShMOLLI) MRI sequences are the sequences of choice for T1 mapping.

However, previous T1 mapping methods, such as MOLLI (65), are based on LL approaches and measure apparent T1 (T1*), which underestimates the true T1 values (65). SMART1 map is a new single-point technique for cardiac T1 mapping. Recently, we compared SMART1 map with MOLLI in an animal model with AMI. SMART1 map yielded higher myocardial T1 values in both normal and infarcted myocardium than MOLLI.

Figure 9 demonstrates the difference in T1 between MI and viable myocardium on both MOLLI and SMART1. At 1.5T magnetic field strength, the inherent T1 value of healthy myocardium is 1,007±30 ms and longer by 30% at 3T 1,220±70 ms, which are substantially shorter than the blood 1,580±130 ms and 1,660±60 ms, respectively (66). Administration of Gd-DTPA substantially reduces the T1 values of infarcted > blood > normal myocardium, but Gd-DTPA relaxivity is not affected by field strength between 1T and 5T. Longer T1 is better for perfusion, T1 mapping and DE-MRI, because it increase the contrast between normal, hypoperfused and MI.

After injection of gadolinium-based MR contrast media (0.1-0.2 mmol/kg), T1 value of the healthy and

© Cardiovascular Diagnosis and Therapy. All rights reserved.

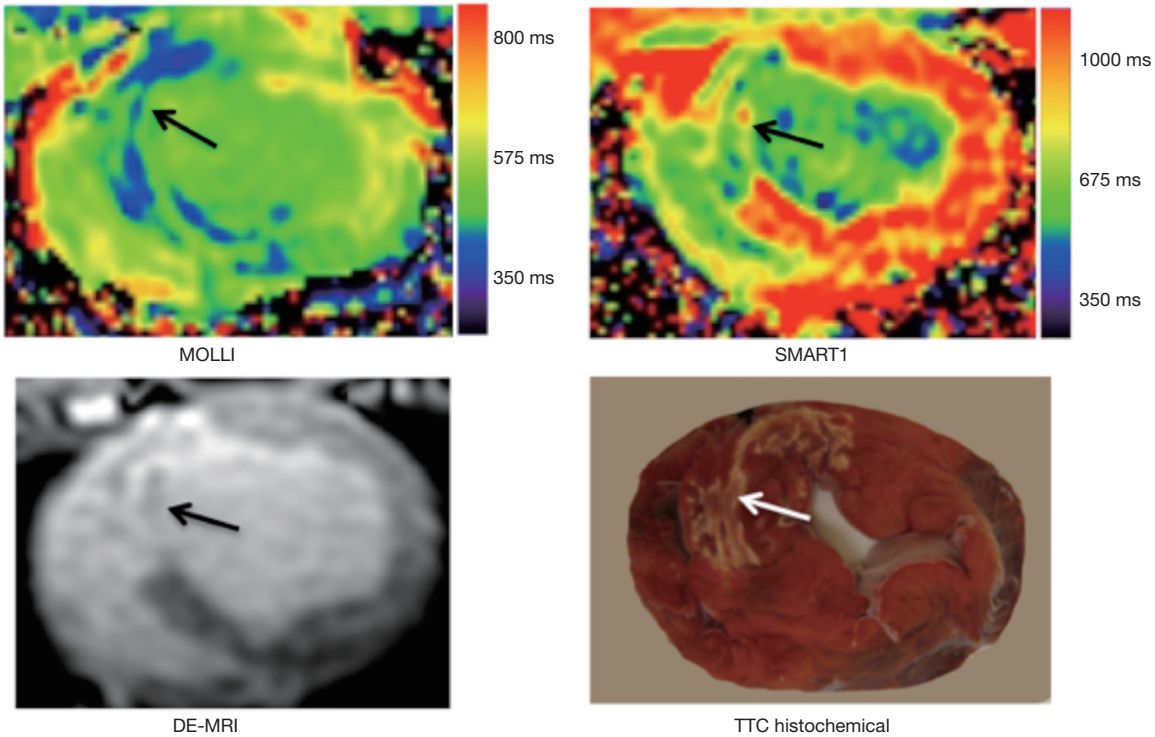

Figure 9 T1 maps (3T) showing the difference in T1 of AMI on MOLLI and SMART1 (arrow). The site of infarct corresponds to DE-MRI and histochemical TTC strain. MOLLI, modified Look-Locker inversion-recovery. AMI, acute myocardial infarct; DE-MRI, Delayed enhancement MRI; TTC, triphenyltetrazolium chloride.

infarcted myocardium differentially decreases followed by continuous increase due to gadolinium washout, with normal myocardium consistently shows a higher T1 than infarcted myocardium or LV cavity (67). Myocardial T1 values that are similar to or lower than the LV cavity blood are indicative of abnormal accumulation of gadolinium in the myocardium (68). It should be noted that contrast enhanced T1 map values are highly dependent on (I) dose of MR contrast media; (II) the time elapsed after contrast media administration; (III) renal clearance of the contrast agent; and (IV) displacement of contrast material by the hematocrit (69). The dose of MR contrast media determines the magnitude of shortening of the T1 relaxation time in myocardium, thus clinical studies should standardize the optimum dose for T1 mapping. It is important to recognize the important of renal clearance of MR contrast media, particularly in patients with chronic renal disease.

T2 mapping

The assessment of myocardial salvage in AMI is clinically important because large salvageable tissue is associated with improved short- and long-term survival after AMI. Furthermore, detection of myocardial edema and salvage can allow for the identification of the infarct-related artery, guide management and act as surrogate end points in clinical trials (70). Detection of myocardial edema, using a dark blood TSE technique, has previously been shown to allow early detection of acute coronary syndromes and may identify both the AAR and myocardial salvage post-reperfusion (71,72). T2-weighted MRI identifies myocardial edema before the onset of irreversible ischemic injury and has shown value in risk-stratifying patients with chest pain. However, several problems inherent to T2-weighted MRI including respiratory/cardiac motion, variability in myocardial signal related to surface coil intensity inhomogeneity and sub-endocardial bright signal derived from slow flowing blood (73,74).

A quantitative T2 relaxation map (T2 mapping) has been introduced in 2007 for quantifying myocardial edema (19,26) and patients with MI (75). Kellman *et al*. found that T2-mapping sequences are superior to T2-weighted sequences

© Cardiovascular Diagnosis and Therapy. All rights reserved.

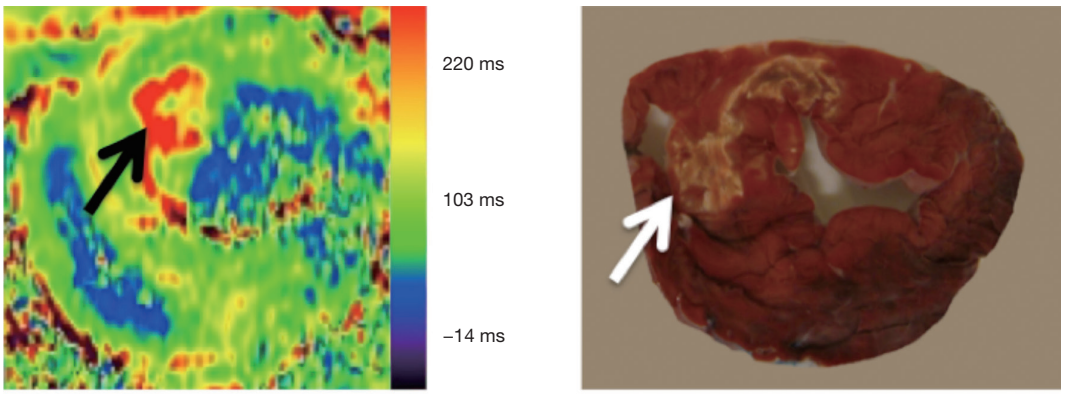

Figure 10 The image shows the difference in T2 between AMI (arrow) and viable myocardium on T2 map. Note the correspondence between the extents of AMI on MRI and histochemical TTC stain. AMI, acute myocardial infarct; TTC, triphenyltetrazolium chloride.

in identifying tissues with interstitial edema (26), because T2-weighted sequences do not offer quantitative T2 measurements that would allow for comparisons between different studies (74). *Figure 10* shows a T2 map of AMI acquire on a 3T scanner.

T2 mapping leverages the increased myocardial free water in the setting of AMI, taking advantage of the positive relationship between T2 signal intensity and tissue water content. After coronary revascularization, there is plasma accumulation in the interstitial and/or intracellular spaces of ischemic myocardium (76,77). It has been reported that T2 signal hyperintensity may identify myocardial ischemia even before detectable injury by troponin or DE-MRI (72). Recent studies showed myocardial T2 relaxation time to increase not only with AMI, but also with severe transient ischemia (18,72). Others found that myocardial T2 is not only determined by an absolute increase in myocardial water, but also by the movement of water molecules from the extracellular to the intracellular spaces and by the dissociation of water molecules from proteins leading to free instead of bound water (78). Hyperintense myocardial regions on T2-weighted images are thought to present edematous AAR of infarction (79-82). These observations have important clinical implications because patients with AAR of infarction are generally expected to benefit from early diagnosis and prompt intervention to arrest the process of cell death.

Recently, Fernández-Jiménez *et al*. (10) described in-depth the time course of myocardial edema in a porcine model of 40 min of coronary artery occlusion followed by reperfusion using T2-map and direct measurements of water content. They demonstrated marked fluctuation in myocardial water: increase in myocardial water content at 2 h of revascularization and substantial drop at 24 h followed by gradual increase after 4 to 7 days. The investigators concluded that the edema is not static, but fluctuates. Thus, this study suggests that investigators testing adjunctive therapies to reduce MI size should be careful about assuming that the zone of edema observed on T2-weighted MRI captures AAR of infarction (72). The edematous region fluctuates over time and may be influenced by therapy. Any therapy that reduces ischemic necrosis may reduce the edematous region in the early hours of coronary revascularization, thus falsely reducing the size of the AAR. Measurement of the edematous region at 24 h, when the early edema has resolved, will also falsely lower the AAR, thus, investigators recommended that anti-inflammatory agents should be tested between 4 to 7 days to determine the benefit of therapy.

Diffusion imaging

Diffusion MRI provides information regarding microscopic tissue structure through encoding random motion (diffusive) of water molecules. Diffusion tensor imaging (DTI) helps to characterize the myocardium and monitoring the process of LV remodeling after AMI (83). An example of microstructure information of an *ex vivo* healthy pig heart obtained with a DTI experiment is given in *Figure 11*. The information includes apparent diffusion coefficient (ADC), fractional anisotropy (FA), and primary diffusion direction weighted by FA.

The earliest applications of cardiac DTI were in characterizing healthy myocardium architecture (84-91).

© Cardiovascular Diagnosis and Therapy. All rights reserved.

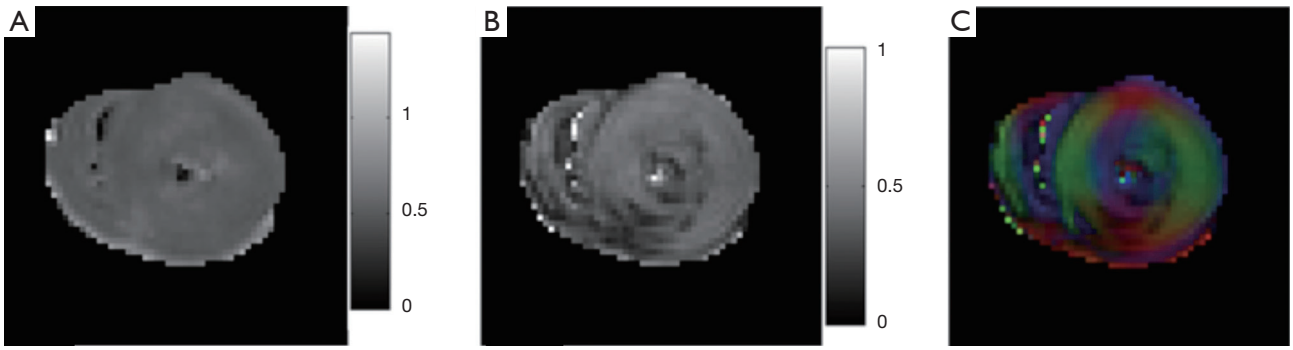

Figure 11 Diffusion parameter maps of an *ex vivo* pig heart: (A) ADC; (B) FA; (C) color-coded FA with red encoding left-right, green encoding up-down, blue encoding in-out directions. ($\times 10^{-3}$ mm^2/s). ADC, apparent diffusion coefficient; FA, fractional anisotropy.

In these studies, the anisotropy property of the diffusion in myocardium was confirmed and the organization of myocardial fiber was observed and verified with histology. Helix angle (HA) maps and fiber tracking of the LV wall showed the transition of the myocardial fibers from right-handed helices to left-handed helices that started in epicardium and ended in endocardium (85-91). Others found during contraction a decrease in subepicardial left-handed helical fibers (LHF) and an increase in subendocardial right-handed helical fibers (RHF) (87). It has also been established that the LV is organized in branching sheet-lets of approximately four-five cardiomyocyte thickness (91-94). The three orthogonal myocytes orientations in the LV are along the local myocyte axis, perpendicular to the local myocyte axis in the sheet-let plane and normal to the sheet-let plane, a structural arrangement known as orthotropy (95). Changes in local myocyte orientation and myolaminar sliding (shearing of adjacent myolaminae over each other) are thought to be the principal mechanisms of ventricular wall thickening in systole (96). The integrity and mobility of these sheet-lets are considered to be fundamental for myocardium function (97). Thus, knowledge of local myocytes and laminar architectures are important in the understanding of normal cardiac function and interpretation of electrical and mechanical studies of cardiac diseases. Investigators also found that myocardial mechanical properties and electrophysiological conductance are different along each orientation (96,98,99). Regarding clinical applications, most of the clinical application studies of DTI are on MI.

Chen *et al*. observed in an *ex vivo* rat hearts the increase in mean diffusivity, decrease in diffusion anisotropy and increase in angular deviation of the primary diffusion direction in scar infarct (100). The increase in mean diffusivity was related to increased extracellular space due to loss of membrane integrity and collagen. Another study showed that the decrease in anisotropy and increase in angular deviation were correlated with microscopic fiber disarray, which has also been found to correlate with viability map (83).

In an *in vivo* swine study, we demonstrated the structural changes in revascularized AMI using DTI. *Figure 12* shows hyperintensity area on T2-weighted images and ADC maps. The area mirrors the increase in regional water content related to MI. The hypointensity areas on FA maps corresponded with hyperenhanced infarct on DE-MRI, but smaller than hyperintensity area on T2-weighted images or ADC maps. The areas with increase ADC, but without a decrease in FA, may reflect salvageable myocardium, while the areas with increase ADC and decrease in FA may represent regions with loss of cellular integrity, which are the cause for enhancement in DE-MRI. Histochemical and histopathological stains show the area risk and infarction.

Wu *et al*. reported infarct zone-dependent changes in ADC, diffusion FA and fiber orientation in patients with 25 days old infarct. ADC data show significant increase, while diffusion anisotropy showed progressive decrease from the infarct and peri-infarct to remote myocardium (83). MI exhibited a substantial loss in the percentage of right-handed helical fibers (% RHF) and an increase in the percentage of left-handed helical fibers (% LHF), while the remote myocardium showed an increase in % RHF and a decrease in % LHF. Furthermore, it was shown that the infarct region with low % LHF correlated well with infarct size.

These aforementioned studies used voxel-by-voxel

© Cardiovascular Diagnosis and Therapy. All rights reserved.

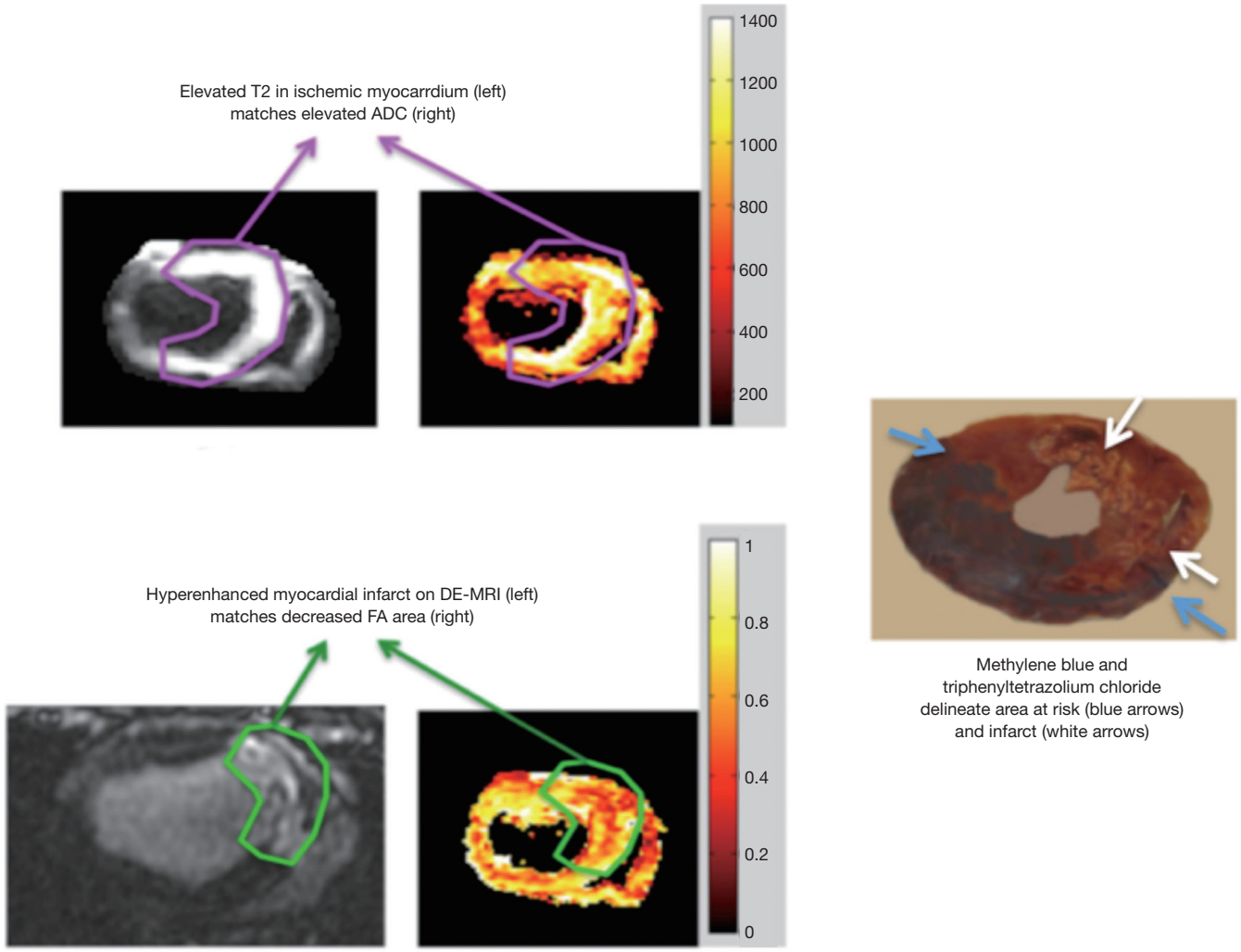

Figure 12 T2-weighted and ADC maps show the correspondence in delineating myocardial infarct (top block), while the hypointensity area on FA maps corresponds with hyperintensity area on DE-MRI (bottom block), but smaller than the hyperintensity areas on T2-weighted or ADC maps. Histochemical methylene blue and TTC stains delineate the area at risk and infarct, respectively. ADC, apparent diffusion coefficient; FA, fractional anisotropy; DE-MRI, Delayed enhancement MRI; TTC, triphenyltetrazolium chloride.

information of the diffusion tensor such as ADC, diffusion anisotropy and HA maps. However, Mekkaoui *et al*. indicated that microstructural reorganization of remodeled LV after AMI can only be fully understood by looking at myofibers as continuous 3D entities (101). Therefore, they introduced statistical tractography-based HA metrics to yield robust measure of 3D myofiber architecture in normal hearts, where they demonstrated in normal hearts positive and negative distribution of HA in subendocardium and subepicardium, respectively. In remote myocardium, a significant shift toward positive HA was found (83,102).

Beside MI, diffusion-weighted imaging (DWI) was applied in hypertrophic cardiomyopathy (97,103,104). One important feature of this disease is myocardial disarray (103). A study by Tseng *et al*. showed significant differences in the mean FA and % HA that are less than –45° between normal (0.75, 6%) and hypertrophied myocardium (0.56, 24%) in patients with hypertrophic cardiomyopathy as evidence of myocardial disarray (104). Additionally, the correlation between diffusion anisotropy and myocardial hypokinesis, measured with strain-rate MRI, was stronger in the cross-fiber direction than fiber direction, implying a connection between fiber disarray and myocardial passive compliance. The angle between principal shortening direction and

© Cardiovascular Diagnosis and Therapy. All rights reserved.

fiber orientation was reported to significantly vary across hypertrophied myocardium, indicating an abnormal transmural coupling.

In a recent study, Ferreira *et al*. reported a larger E2A, which is the angle of the second eigenvector of diffusion relative to the local wall tangent plane, in systole than in diastole in control group (97). This finding is consistent with previously reported changes of transmural angulation of the sheet-let structure (97). The same study reported that E2A of hypertrophied hearts retaining similar value during systolic as during diastolic, which implies impaired sheet-let mobility. The abnormal retaining of E2A values was shown to be associate with increased wall thickness but not with the presence of scar infarct on DE-MRI. Evidence of significantly greater contraction in hypertrophied hearts was shown through the increased E2A values in both systole (63.9° *vs*. 56.4° healthy volunteers) and diastole (46.8° *vs*. 24° healthy volunteers).

With the increased maturity of acquisition and post-processing techniques, cardiac DTI is gaining momentum and providing more insights to diagnosis and prognosis of myocardial diseases. Cardiac DTI has the potential to characterize structural changes extending beyond infarct areas such as myocyte death (apoptosis), scar formation, myocyte hypertrophy, fiber disarray, angiogenesis, and diffuse fibrosis (100). Thus, with DTI of myocardium, we cross the barrier of pure morphological imaging and move on to microstructural and functional imaging. Furthermore, a clinical study showed that DWI has the potential to detect MI in 78% of patients in less than 1 minute acquisition time, with a similar extent as on DE-MRI (105). Thus, investigators suggested the use DWI in emergency patients with atypical chest pain for confirming/denying the presence of AMI in a few minutes and for differentiating acute from scar infarct. Laissy *et al*. (105) recently investigated the clinical feasibility of DWI in detecting AMI and to differentiate it from subacute and chronic MI, with delayed contrast enhancement MRI sequence as reference. Furthermore, they measured the variation of the myocardial ADC according to the age of MI. They found that qualitative assessment of DWI compared with delayed contrast enhancement images yielded a sensitivity of 97% and a specificity of 61%/14% to differentiate acute from chronic/subacute MI, respectively. The absolute ADCs (acute $=0.00632 \pm 0.00037$ mm^2/s, subacute $=0.00639 \pm 0.00035$ mm^2/s, chronic $=0.00743 \pm 0.00056$ mm^2/s, remote or normal $=0.00895 \pm 0.00019$ mm^2/s) and relative ADCs were significantly different between groups ($P<0.001$) except between AMI and subacute. This study shows that DWI is a sensitive technique to diagnose recent MI. DWI MR Sequences could help differentiate recent from chronic MI.

Hybrid imaging

Novel trends in hybrid imaging, such as cardiac PET/MRI and optical imaging/MRI, are recently under intensive investigation. For example, it has been shown in patients with chronic ischemic heart disease that FDG PET can differentiate viable myocardium from scar. However, in patients with AMI, FDG-PET is unreliable for the assessment of myocardial viability because reduced glucose uptake has also been observed in reperfused ischemic (stunned or hibernating) myocardium, resulting in overestimation of infarct size (106-109). On PET/MRI, the area of reduced FDG uptake was shown to correspond to the area of myocardial edema in a patient with reperfused AMI, which, in turn, has been demonstrated to delineate the AAR (72,108). Therefore, we hypothesized that reduced myocardial FDG uptake allows for the delineation of the AAR in patients with reperfused AMI. Nensa *et al*. (110) found in patients with infarcted myocardium and reduced FDG uptake, a good correlation between the area of reduced FDG uptake and the AAR ($r=0.70$, $P=0.001$). The area of reduced FDG uptake (31%±11% LV mass) was larger than the infarct size (10%±10%, $P<0.0001$) and the AAR (17%±13%, $P<0.0001$). In six out of 18 patients, no late contrast enhancement was seen, whereas all patients had an area of reduced FDG uptake (29%±8%) in the perfusion territory of the culprit artery. They concluded that in patients with reperfused AMI, the area of reduced FDG uptake correlates with the AAR and is localized in the perfusion territory of the culprit artery in the absence of necrosis, although the area of reduced FDG uptake largely overestimates the infarct size and AAR.

MRI-guided procedures

In the last decade MRI has been extended from a diagnostic to dynamic modality by tracking intravascular guide-wires and catheters in real-time (111). MRI-guided interventions became possible because of major advancements in the speed of data acquisition, data transfer, interactive control-display, highly uniform magnetic fields, rapidly changeable magnetic field gradients, multi-channel receivers and computing systems. Open and closed bore MR scanners have been used for cardiovascular interventions (112).

© Cardiovascular Diagnosis and Therapy. All rights reserved.

Open scanners were designed to ease patient access/observation and increase comfort for the interventionists. Multiple venders have recently introduced hybrid systems (combination of X-ray fluoroscopy or PET with MRI). These systems can be used for detecting and characterizing the disease prior to intervention, provide guidance during intervention and monitor the progress of treatment.

MRI-guidance has been frequently used for stenting of the aorta, pulmonary, coronary, renal, iliac and femoral arteries (113-118). MRI-guided coronary artery stent placement, however, is a challenging interventional procedure because of the small size of the coronary arteries combined with incessant motion during the respiratory and cardiac cycles. These obstacles necessitate higher temporal and spatial resolution for real-time MRI when compared with interventional peripheral MR angiography (118). Bock *et al*. described in detail the technical prerequisites for MRI-guided endovascular interventions and addressed the safety aspects of this technique (119).

Pre-clinical studies indicated that cell transplantation, delivered under MRI-guidance, is safe and feasible (120-122). Stem cell tracking on MRI is based on labeling injected cells with FDA approved super paramagnetic iron oxide particles. Weeks later, MRI examination showed the increase in collateral blood flow of infarcted myocardium after delivering vascular endothelial growth gene (121). Intramyocardial delivery of gene therapy has been also performed under MRI-guidance (123-125). The advancement of molecular and metabolic imaging will improve diagnostic accuracy and allow patient-specific targeted therapy, designed to maximize disease control and minimize side effects. The advancement of molecular and cellular therapies with MRI-guided targeted procedure will open new avenue in patient-specific targeted therapy in the future.

Future perspectives

MRI guided interventions have also been performed in patients with congenital heart diseases including for the placement of transjugular catheters and cardiac catheterization, as well as repair of aortic coarctation and atrio-septal defects. This minimally invasive technique has been used for closure of atrio-septal defects and local drug delivery (126-129). Currently, there is great interest to develop a catheter based MRI-guided high-intensity focused ultrasound (HIFU) for ablating the sites causing ventricular arrhythmia. The catheter tip creates an ablative energy source (heat) that can precisely penetrate into the target without affecting surrounding tissues. It also provides real-time anatomic and thermal mapping of targeted tissue (130). Clinical studies showed atrial scar on DE-MRI after HIFU (131-133).

Conclusions

It can be concluded that MRI has revolutionized cardiac imaging. MRI gives complementary information on LV function, regional perfusion, angiogenesis, myocardial viability and local orientations of myocytes and their arrays. Recent advances in cardiac imaging include T1 mapping, T2 mapping (for myocardial viability), diffusion imaging (for myocardial architecture) and MR-guided interventions (for delivery of local therapies and ablation). Diffusion MRI provides information regarding microscopic tissue structure, while DTI helps characterizing the myocardium and monitoring the process of LV remodeling after AMI. MR-guided intervention is another young and rapidly evolving field. With the promise of higher spatial-temporal resolution and 3D coverage, in the near future, cardiac MRI will be an indispensible tool in the diagnosis of cardiac diseases, coronary intervention and myocardial therapeutic delivery.

Acknowledgements

None.

Footnote

Conflicts of Interest: The authors have no conflicts of interest to declare.

References

1. Chan J, Khafagi F, Young AA, et al. Impact of coronary revascularization and transmural extent of scar on regional left ventricular remodelling. Eur Heart J 2008;29:1608-17.
2. Gutberlet M, Fröhlich M, Mehl S, et al. Myocardial viability assessment in patients with highly impaired left ventricular function: Comparison of delayed enhancement, dobutamine stress mri, end-diastolic wall thickness, and ti201-spect with functional recovery after revascularization. Eur Radiol 2005;15:872-80.
3. Mahrholdt H, Wagner A, Parker M, et al. Relationship of contractile function to transmural extent of infarction in patients with chronic coronary artery disease. J Am Coll

© Cardiovascular Diagnosis and Therapy. All rights reserved.

Cardiol 2003;42:505-12.
4. Einstein AJ, Berman DS, Min JK, et al. Patient-centered imaging: shared decision making for cardiac imaging procedures with exposure to ionizing radiation. J Am Coll Cardiol 2014;63:1480-9.
5. Meyer GP, Wollert KC, Lotz J, et al. Intracoronary bone marrow cell transfer after myocardial infarction: eighteen months' follow-up data from the randomized, controlled BOOST (Bone marrow transfer to enhance ST-elevation infarct regeneration) trial. Circulation 2006;113:1287-94.
6. Schächinger V, Assmus B, Britten MB, et al. Transplantation of progenitor cells and regeneration enhancement in acute myocardial infarction: Final one-year results of the TOPCARE-AMI trial. J Am Coll Cardiol 2004;44:1690-9.
7. Burns RJ, Gibbons RJ, Yi Q, et al. The relationships of left ventricular ejection fraction, end-systolic volume index and infarct size to six-month mortality after hospital discharge following myocardial infarction treated by thrombolysis. J Am Coll Cardiol 2002;39:30-6.
8. Ørn S, Manhenke C, Greve OJ, et al. Microvascular obstruction is a major determinant of infarct healing and subsequent left ventricular remodelling following primary percutaneous coronary intervention. Eur Heart J 2009;30:1978-85.
9. Olimulder MA, Galjee MA, Wagenaar LJ, et al. Relationship between infarct tissue characteristics and left ventricular remodeling in patients with versus without early revascularization for acute myocardial infarction as assessed with contrast-enhanced cardiovascular magnetic resonance imaging. Int Heart J 2012;53:263-9.
10. Fernández-Jiménez R, Sánchez-González J, Agüero J, et al. Myocardial edema after ischemia/reperfusion is not stable and follows a bimodal pattern: Imaging and histological tissue characterization. J Am Coll Cardiol 2015;65:315-23.
11. Arheden H, Saeed M, Higgins CB, et al. Reperfused rat myocardium subjected to various durations of ischemia: Estimation of the distribution volume of contrast material with echo-planar MR imaging. Radiology 2000;215:520-8.
12. Sutton MG, Sharpe N. Left ventricular remodeling after myocardial infarction: Pathophysiology and therapy. Circulation 2000;101:2981-8.
13. Kallianos K, Moraes GL, Ordovas KG. Prognostic role of MR imaging in nonischemic myocardial disease. Magn Reson Imaging Clin N Am 2015;23:89-94.
14. Kathiria NN, Higgins CB, Ordovas KG. Advances in MR imaging assessment of adults with congenital heart disease. Magn Reson Imaging Clin N Am 2015;23:35-40.
15. Kohi MP, Ordovas KG, Naeger DM, et al. CMR assessment of right ventricular function in patients with combined pulmonary stenosis and insufficiency after correction of tetralogy of Fallot. Acta Radiol 2013;54:1132-7.
16. Naeger DM, Higgins C, De Marco T, et al. Low-intensity late gadolinium enhancement predominates in hypertrophic cardiomyopathy. Clin Imaging 2015;39:432-6.
17. Heidemann RM, Ozsarlak O, Parizel PM, et al. A brief review of parallel magnetic resonance imaging. Eur Radiol 2003;13:2323-37.
18. Abdel-Aty H, Simonetti O, Friedrich MG. T2-weighted cardiovascular magnetic resonance imaging. J Magn Reson Imaging 2007;26:452-9.
19. Giri S, Chung YC, Merchant A, et al. T2 quantification for improved detection of myocardial edema. J Cardiovasc Magn Reson 2009;11:56.
20. Leithner C, Gertz K, Schröck H, et al. A flow sensitive alternating inversion recovery (FAIR)-MRI protocol to measure hemispheric cerebral blood flow in a mouse stroke model. Exp Neurol 2008;210:118-27.
21. Théberge J. Perfusion magnetic resonance imaging in psychiatry. Top Magn Reson Imaging 2008;19:111-30.
22. Detre JA, Alsop DC. Perfusion magnetic resonance imaging with continuous arterial spin labeling: Methods and clinical applications in the central nervous system. Eur J Radiol 1999;30:115-24.
23. Moffat BA, Chenevert TL, Hall DE, et al. Continuous arterial spin labeling using a train of adiabatic inversion pulses. J Magn Reson Imaging 2005;21:290-6.
24. Vandsburger MH, Janiczek RL, Xu Y, et al. Improved arterial spin labeling after myocardial infarction in mice using cardiac and respiratory gated look-locker imaging with fuzzy c-means clustering. Magn Reson Med 2010;63:648-57.
25. Wang X, Hu Q, Mansoor A, et al. Bioenergetic and functional consequences of stem cell-based vegf delivery in pressure-overloaded swine hearts. Am J Physiol Heart Circ Physiol 2006;290:H1393-405.
26. Kellman P, Arai AE. Imaging sequences for first pass perfusion--a review. J Cardiovasc Magn Reson 2007;9:525-37.
27. Greenwood JP, Maredia N, Younger JF, et al. Cardiovascular magnetic resonance and single-photon emission computed tomography for diagnosis of coronary heart disease (CE-MARC): a prospective trial. Lancet 2012;379:453-60.

© Cardiovascular Diagnosis and Therapy. All rights reserved.

28. Gutberlet M, Noeske R, Schwinge K, et al. Comprehensive cardiac magnetic resonance imaging at 3.0 tesla: Feasibility and implications for clinical applications. Invest Radiol 2006;41:154-67.
29. Araoz PA, Glockner JF, McGee KP, et al. 3 Tesla MR imaging provides improved contrast in first-pass myocardial perfusion imaging over a range of gadolinium doses. J Cardiovasc Magn Reson 2005;7:559-64.
30. Di Bella EV, Parker DL, Sinusas AJ. On the dark rim artifact in dynamic contrast-enhanced MRI myocardial perfusion studies. Magn Reson Med 2005;54:1295-9.
31. Christian TF, Bell SP, Whitesell L, et al. Accuracy of cardiac magnetic resonance of absolute myocardial blood flow with a high-field system: comparison with conventional field strength. JACC Cardiovasc Imaging 2009;2:1103-10.
32. Gupta A, Lee VS, Chung YC, et al. Myocardial infarction: Optimization of inversion times at delayed contrast-enhanced MR imaging. Radiology 2004;233:921-6.
33. Klumpp B, Fenchel M, Hoevelborn T, et al. Assessment of myocardial viability using delayed enhancement magnetic resonance imaging at 3.0 Tesla. Invest Radiol 2006;41:661-7.
34. Ligabue G, Fiocchi F, Ferraresi S, et al. 3-Tesla MRI for the evaluation of myocardial viability: A comparative study with 1.5-Tesla MRI. Radiol Med 2008;113:347-62.
35. Ibrahim T, Bulow HP, Hackl T, et al. Diagnostic value of contrast-enhanced magnetic resonance imaging and single-photon emission computed tomography for detection of myocardial necrosis early after acute myocardial infarction. J Am Coll Cardiol 2007;49:208-16.
36. Kim RJ, Albert TS, Wible JH, et al. Performance of delayed-enhancement magnetic resonance imaging with gadoversetamide contrast for the detection and assessment of myocardial infarction: An international, multicenter, double-blinded, randomized trial. Circulation 2008;117:629-37.
37. Kaandorp TA, Lamb HJ, Poldermans D, et al. Assessment of right ventricular infarction with contrast-enhanced magnetic resonance imaging. Coron Artery Dis 2007;18:39-43.
38. Kim RJ, Wu E, Rafael A, et al. The use of contrast-enhanced magnetic resonance imaging to identify reversible myocardial dysfunction. N Engl J Med 2000;343:1445-53.
39. Saeed M, Hetts SW, Do L, et al. MRI study on volume effects of coronary emboli on myocardial function, perfusion and viability. Int J Cardiol 2013;165:93-9.
40. Saeed M, Hetts SW, Do L, et al. Coronary microemboli effects in preexisting acute infarcts in a swine model: cardiac MR imaging indices, injury biomarkers, and histopathologic assessment. Radiology 2013;268:98-108.
41. Kumar A, Abdel-Aty H, Kriedemann I, et al. Contrast-enhanced cardiovascular magnetic resonance imaging of right ventricular infarction. J Am Coll Cardiol 2006;48:1969-76.
42. Arheden H, Saeed M, Higgins CB, et al. Measurement of the distribution volume of gadopentetate dimeglumine at echo-planar MR imaging to quantify myocardial infarction: Comparison with 99m Tc-DTPA autoradiography in rats. Radiology 1999;211:698-708.
43. Saeed M, Lund G, Wendland MF, et al. Magnetic resonance characterization of the peri-infarction zone of reperfused myocardial infarction with necrosis-specific and extracellular nonspecific contrast media. Circulation 2001;103:871-6.
44. Rubenstein JC, Lee DC, Wu E, et al. A comparison of cardiac magnetic resonance imaging peri-infarct border zone quantification strategies for the prediction of ventricular tachyarrhythmia inducibility. Cardiol J 2013;20:68-77.
45. Yan AT, Shayne AJ, Brown KA, et al. Characterization of the peri-infarct zone by contrast-enhanced cardiac magnetic resonance imaging is a powerful predictor of post-myocardial infarction mortality. Circulation 2006;114:32-9.
46. Wu E, Ortiz JT, Tejedor P, et al. Infarct size by contrast enhanced cardiac magnetic resonance is a stronger predictor of outcomes than left ventricular ejection fraction or end-systolic volume index: prospective cohort study. Heart 2008;94:730-6.
47. Roes SD, Kelle S, Kaandorp TA, et al. Comparison of myocardial infarct size assessed with contrast-enhanced magnetic resonance imaging and left ventricular function and volumes to predict mortality in patients with healed myocardial infarction. Am J Cardiol 2007;100:930-6.
48. Masci PG, Ganame J, Strata E, et al. Myocardial salvage by CMR correlates with LV remodeling and early ST-segment resolution in acute myocardial infarction. JACC Cardiovasc Imaging 2010;3:45-51.
49. Cummings KW, Bhalla S, Javidan-Nejad C, et al. A pattern-based approach to assessment of delayed enhancement in nonischemic cardiomyopathy at MR imaging. Radiographics 2009;29:89-103.
50. Ahmed N, Carrick D, Layland J, et al. The role of cardiac magnetic resonance imaging (MRI) in acute myocardial

© Cardiovascular Diagnosis and Therapy. All rights reserved.

infarction (AMI). Heart Lung Circ 2013;22:243-55.
51. Wu KC, Kim RJ, Bluemke DA, et al. Quantification and time course of microvascular obstruction by contrast-enhanced echocardiography and magnetic resonance imaging following acute myocardial infarction and reperfusion. J Am Coll Cardiol 1998;32:1756-64.
52. Pislaru SV, Barrios L, Stassen T, et al. Infarct size, myocardial hemorrhage, and recovery of function after mechanical versus pharmacological reperfusion: Effects of lytic state and occlusion time. Circulation 1997;96:659-66.
53. van Gaal WJ, Banning AP. Percutaneous coronary intervention and the no-reflow phenomenon. Expert Rev Cardiovasc Ther 2007;5:715-31.
54. Wu KC. CMR of microvascular obstruction and hemorrhage in myocardial infarction. J cardiovasc Magn Reson 2012;14:68.
55. Saeed M, Wendland MF, Yu KK, et al. Identification of myocardial reperfusion with echo planar magnetic resonance imaging. Discrimination between occlusive and reperfused infarctions. Circulation 1994;90:1492-501.
56. Schmidt A, Azevedo CF, Cheng A, et al. Infarct tissue heterogeneity by magnetic resonance imaging identifies enhanced cardiac arrhythmia susceptibility in patients with left ventricular dysfunction. Circulation 2007;115:2006-14.
57. Bajwa HZ, Do L, Suhail M, et al. MRI demonstrates a decrease in myocardial infarct healing and increase in compensatory ventricular hypertrophy following mechanical microvascular obstruction. J Magn Reson Imaging 2014;40:906-14.
58. Fieno DS, Hillenbrand HB, Rehwald WG, et al. Infarct resorption, compensatory hypertrophy, and differing patterns of ventricular remodeling following myocardial infarctions of varying size. J Am Coll Cardiol 2004;43:2124-31.
59. Ganame J, Messalli G, Masci PG, et al. Time course of infarct healing and left ventricular remodelling in patients with reperfused ST segment elevation myocardial infarction using comprehensive magnetic resonance imaging. Eur Radiol 2011;21:693-701.
60. Lund GK, Stork A, Muellerleile K, et al. Prediction of left ventricular remodeling and analysis of infarct resorption in patients with reperfused myocardial infarcts by using contrast-enhanced MR imaging. Radiology 2007;245:95-102.
61. Pokorney SD, Rodriguez JF, Ortiz JT, et al. Infarct healing is a dynamic process following acute myocardial infarction. J cardiovasc Magn Reson 2012;14:62.
62. Iles L, Pfluger H, Phrommintikul A, et al. Evaluation of diffuse myocardial fibrosis in heart failure with cardiac magnetic resonance contrast-enhanced T1 mapping. J Am Coll Cardiol 2008;52:1574-80.
63. Karmonik C, Malaty A, Bikram M, et al. Fast in vivo quantification of T1 and T2 MRI relaxation times in the myocardium based on inversion recovery SSFP with in vitro validation post gd-based contrast administration. Cardiovasc Diagn Ther 2014;4:88-96.
64. Schmitt P, Griswold MA, Jakob PM, et al. Inversion recovery True FISP: quantification of T(1), T(2), and spin density. Magn Reson Med 2004;51:661-7.
65. Messroghli DR, Greiser A, Fröhlich M, et al. Optimization and validation of a fully-integrated pulse sequence for modified look-locker inversion-recovery (MOLLI) T1 mapping of the heart. J Magn Reson Imaging 2007;26:1081-6.
66. Sharma P, Socolow J, Patel S, et al. Effect of Gd-DTPA-BMA on blood and myocardial T1 at 1.5T and 3T in humans. J Magn Reson Imaging 2006;23:323-30.
67. Saeed M, Higgins CB, Geschwind JF, et al. T1-relaxation kinetics of extracellular, intracellular and intravascular MR contrast agents in normal and acutely reperfused infarcted myocardium using echo-planar MR imaging. Eur Radiol 2000;10:310-8.
68. Geschwind JF, Saeed M, Wendland MF, et al. Depiction of reperfused myocardial infarction using contrast-enhanced spin echo and gradient echo magnetic resonance imaging. Invest Radiol 1998;33:386-92.
69. Mongeon FP, Jerosch-Herold M, Coelho-Filho OR, et al. Quantification of extracellular matrix expansion by CMR in infiltrative heart disease. JACC Cardiovasc Imaging 2012;5:897-907.
70. Desch S, Eitel I, de Waha S, et al. Cardiac magnetic resonance imaging parameters as surrogate endpoints in clinical trials of acute myocardial infarction. Trials 2011;12:204.
71. Abdel-Aty H, Cocker M, Meek C, et al. Edema as a very early marker for acute myocardial ischemia: A cardiovascular magnetic resonance study. J Am Coll Cardiol 2009;53:1194-201.
72. Aletras AH, Tilak GS, Natanzon A, et al. Retrospective determination of the area at risk for reperfused acute myocardial infarction with T2-weighted cardiac magnetic resonance imaging: Histopathological and displacement encoding with stimulated echoes (DENSE) functional validations. Circulation 2006;113:1865-70.
73. Arai AE. Using magnetic resonance imaging to

© Cardiovascular Diagnosis and Therapy. All rights reserved.

characterize recent myocardial injury: utility in acute coronary syndrome and other clinical scenarios. Circulation 2008;118:795-6.
74. Pennell D. Myocardial salvage: retrospection, resolution, and radio waves. Circulation 2006;113:1821-3.
75. Verhaert D, Thavendiranathan P, Giri S, et al. Direct T2 quantification of myocardial edema in acute ischemic injury. JACC Cardiovasc Imaging 2011;4:269-78.
76. Bragadeesh T, Jayaweera AR, Pascotto M, et al. Post-ischaemic myocardial dysfunction (stunning) results from myofibrillar oedema. Heart 2008;94:166-71.
77. Turschner O, D'Hooge J, Dommke C, et al. The sequential changes in myocardial thickness and thickening which occur during acute transmural infarction, infarct reperfusion and the resultant expression of reperfusion injury. Eur Heart J 2004;25:794-803.
78. Friedrich MG. Myocardial edema--a new clinical entity? Nat Rev Cardiol 2010;7:292-6.
79. Berry C, Kellman P, Mancini C, et al. Magnetic resonance imaging delineates the ischemic area at risk and myocardial salvage in patients with acute myocardial infarction. Circ Cardiovasc Imaging 2010;3:527-35.
80. Croisille P, Revel D, Saeed M. Contrast agents and cardiac MR imaging of myocardial ischemia: From bench to bedside. Eur Radiol 2006;16:1951-63.
81. Ibanez B, Macaya C, Sánchez-Brunete V, et al. Effect of early metoprolol on infarct size in ST-segment-elevation myocardial infarction patients undergoing primary percutaneous coronary intervention: The Effect of Metoprolol in Cardioprotection During an Acute Myocardial Infarction (METOCARD-CNIC) trial. Circulation 2013;128:1495-503.
82. Saeed M, Martin AJ, Saloner D, et al. Noninvasive MR characterization of structural and functional components of reperfused infarct. Acta Radiol 2010;51:1093-102.
83. Wu MT, Tseng WY, Su MY, et al. Diffusion tensor magnetic resonance imaging mapping the fiber architecture remodeling in human myocardium after infarction: correlation with viability and wall motion. Circulation 2006;114:1036-45.
84. Edelman RR, Gaa J, Wedeen VJ, et al. In vivo measurement of water diffusion in the human heart. Magn Reson Med 1994;32:423-8.
85. Tseng WY, Wedeen VJ, Reese TG, et al. Diffusion tensor MRI of myocardial fibers and sheets: correspondence with visible cut-face texture. J Magn Reson Imaging 2003;17:31-42.
86. Sosnovik DE, Wang R, Dai G, et al. Diffusion MR tractography of the heart. J Cardiovasc Magn Reson 2009;11:47.
87. Hales PW, Schneider JE, Burton RA, et al. Histo-anatomical structure of the living isolated rat heart in two contraction states assessed by diffusion tensor MRI. Prog Biophys Mol Biol 2012;110:319-30.
88. Garrido L, Wedeen VJ, Kwong KK, et al. Anisotropy of water diffusion in the myocardium of the rat. Circ Res 1994;74:789-93.
89. Reese TG, Weisskoff RM, Smith RN, et al. Imaging myocardial fiber architecture in vivo with magnetic resonance. Magn Reson Med 1995;34:786-91.
90. Holmes AA, Scollan DF, Winslow RL. Direct histological validation of diffusion tensor MRI in formaldehyde-fixed myocardium. Magn Reson Med 2000;44:157-61.
91. Scollan DF, Holmes A, Winslow R, et al. Histological validation of myocardial microstructure obtained from diffusion tensor magnetic resonance imaging. Am J Physiol 1998;275:H2308-18.
92. LeGrice IJ, Smaill BH, Chai LZ, et al. Laminar structure of the heart: ventricular myocyte arrangement and connective tissue architecture in the dog. Am J Physiol 1995;269:H571-82.
93. Helm P, Beg MF, Miller MI, et al. Measuring and mapping cardiac fiber and laminar architecture using diffusion tensor mr imaging. Ann N Y Acad Sci 2005;1047:296-307.
94. Helm PA, Tseng HJ, Younes L, et al. Ex vivo 3D diffusion tensor imaging and quantification of cardiac laminar structure. Magn Reson Med 2005;54:850-9.
95. Bernus O, Radjenovic A, Trew ML, et al. Comparison of diffusion tensor imaging by cardiovascular magnetic resonance and gadolinium enhanced 3d image intensity approaches to investigation of structural anisotropy in explanted rat hearts. J Cardiovasc Magn Reson 2015;17:31.
96. Gilbert SH, Benson AP, Li P, et al. Regional localisation of left ventricular sheet structure: Integration with current models of cardiac fibre, sheet and band structure. Eur J Cardiothorac Surg 2007;32:231-49.
97. Ferreira PF, Kilner PJ, McGill LA, et al. In vivo cardiovascular magnetic resonance diffusion tensor imaging shows evidence of abnormal myocardial laminar orientations and mobility in hypertrophic cardiomyopathy. J Cardiovasc Magn Reson 2014;16:87.
98. Caldwell BJ, Trew ML, Sands GB, et al. Three distinct directions of intramural activation reveal nonuniform side-to-side electrical coupling of ventricular myocytes. Circ Arrhythm Electrophysiol 2009;2:433-40.
99. Hooks DA, Trew ML, Caldwell BJ, et al. Laminar

© Cardiovascular Diagnosis and Therapy. All rights reserved.

arrangement of ventricular myocytes influences electrical behavior of the heart. Circ Res 2007;101:e103-12.
100. Chen J, Song SK, Liu W, et al. Remodeling of cardiac fiber structure after infarction in rats quantified with diffusion tensor MRI. Am J Physiol Heart Circ Physiol 2003;285:H946-54.
101. Mekkaoui C, Huang S, Chen HH, et al. Fiber architecture in remodeled myocardium revealed with a quantitative diffusion CMR tractography framework and histological validation. J Cardiovasc Magn Reson 2012;14:70.
102. Wu MT, Su MY, Huang YL, et al. Sequential changes of myocardial microstructure in patients postmyocardial infarction by diffusion-tensor cardiac MR: Correlation with left ventricular structure and function. Circ Cardiovasc Imaging 2009;2:32-40, 6 p following 40.
103. McGill LA, Ismail TF, Nielles-Vallespin S, et al. Reproducibility of in-vivo diffusion tensor cardiovascular magnetic resonance in hypertrophic cardiomyopathy. J Cardiovasc Magn Reson 2012;14:86.
104. Tseng WY, Dou J, Reese TG, et al. Imaging myocardial fiber disarray and intramural strain hypokinesis in hypertrophic cardiomyopathy with MRI. J Magn Reson Imaging 2006;23:1-8.
105. Laissy JP, Gaxotte V, Ironde-Laissy E, et al. Cardiac diffusion-weighted MR imaging in recent, subacute, and chronic myocardial infarction: a pilot study. J Magn Reson Imaging 2013;38:1377-87.
106. Fukuoka Y, Nakano A, Uzui H, et al. Reverse blood flow-glucose metabolism mismatch indicates preserved oxygen metabolism in patients with revascularised myocardial infarction. Eur J Nucl Med Mol Imaging 2013;40:1155-62.
107. Di Carli MF, Prcevski P, Singh TP, et al. Myocardial blood flow, function, and metabolism in repetitive stunning. J Nucl Med 2000;41:1227-34.
108. Nensa F, Mahabadi AA, Erbel R, et al. Myocardial edema during acute myocardial infarction visualized by diffusion-weighted MRI. Herz 2013;38:509-10.
109. Nensa F, Poeppel TD, Beiderwellen K, et al. Hybrid PET/MR imaging of the heart: feasibility and initial results. Radiology 2013;268:366-73.
110. Nensa F, Poeppel T, Tezgah E, et al. Integrated FDG PET/MR Imaging for the Assessment of Myocardial Salvage in Reperfused Acute Myocardial Infarction. Radiology 2015;276:400-7.
111. Saeed M, Martin A, Ursell P, et al. MR assessment of myocardial perfusion, viability, and function after intramyocardial transfer of VM202, a new plasmid human hepatocyte growth factor in ischemic swine myocardium. Radiology 2008;249:107-18.
112. Hushek SG, Martin AJ, Steckner M, et al. MR systems for MRI-guided interventions. J Magn Reson Imaging 2008;27:253-66.
113. Kuehne T, Saeed M, Higgins CB, et al. Endovascular stents in pulmonary valve and artery in swine: Feasibility study of MR imaging-guided deployment and postinterventional assessment. Radiology 2003;226:475-81.
114. Omary RA, Frayne R, Unal O, et al. MR-guided angioplasty of renal artery stenosis in a pig model: a feasibility study. J Vasc Interv Radiol 2000;11:373-81.
115. Paetzel C, Zorger N, Bachthaler M, et al. Magnetic resonance-guided percutaneous angioplasty of femoral and popliteal artery stenoses using real-time imaging and intra-arterial contrast-enhanced magnetic resonance angiography. Invest Radiol 2005;40:257-62.
116. Saeed M, Henk CB, Weber O, et al. Delivery and assessment of endovascular stents to repair aortic coarctation using mr and x-ray imaging. J Magn Reson Imaging 2006;24:371-8.
117. Buecker A, Neuerburg JM, Adam GB, et al. Real-time MR fluoroscopy for MR-guided iliac artery stent placement. J Magn Reson Imaging 2000;12:616-22.
118. Spuentrup E, Ruebben A, Schaeffter T, et al. Magnetic resonance--guided coronary artery stent placement in a swine model. Circulation 2002;105:874-9.
119. Bock M, Wacker FK. MR-guided intravascular interventions: techniques and applications. J Magn Reson Imaging 2008;27:326-38.
120. Dick AJ, Guttman MA, Raman VK, et al. Magnetic resonance fluoroscopy allows targeted delivery of mesenchymal stem cells to infarct borders in Swine. Circulation 2003;108:2899-904.
121. Ebert SN, Taylor DG, Nguyen HL, et al. Noninvasive tracking of cardiac embryonic stem cells in vivo using magnetic resonance imaging techniques. Stem Cells 2007;25:2936-44.
122. Hill JM, Dick AJ, Raman VK, et al. Serial cardiac magnetic resonance imaging of injected mesenchymal stem cells. Circulation. 2003;108:1009-14.
123. Carlsson M, Osman NF, Ursell PC, et al. Quantitative MR measurements of regional and global left ventricular function and strain after intramyocardial transfer of VM202 into infarcted swine myocardium. Am J Physiol Heart Circ Physiol 2008;295:H522-32.
124. Jacquier A, Higgins CB, Martin AJ, et al. Injection of adeno-associated viral vector encoding vascular endothelial growth factor gene in infarcted swine myocardium: MR

© Cardiovascular Diagnosis and Therapy. All rights reserved.

measurements of left ventricular function and strain. Radiology 2007;245:196-205.
125. Saeed M, Martin A, Jacquier A, et al. Permanent coronary artery occlusion: Cardiovascular MR imaging is platform for percutaneous transendocardial delivery and assessment of gene therapy in canine model. Radiology 2008;249:560-71.
126. Assmus B, Honold J, Schächinger V, et al. Transcoronary transplantation of progenitor cells after myocardial infarction. N Engl J Med 2006;355:1222-32.
127. Freyman T, Polin G, Osman H, et al. A quantitative, randomized study evaluating three methods of mesenchymal stem cell delivery following myocardial infarction. Eur Heart J 2006;27:1114-22.
128. Menasché P, Alfieri O, Janssens S, et al. The Myoblast Autologous Grafting in Ischemic Cardiomyopathy (MAGIC) trial: first randomized placebo-controlled study of myoblast transplantation. Circulation 2008;117:1189-200.
129. Saito T, Kuang JQ, Lin CC, et al. Transcoronary implantation of bone marrow stromal cells ameliorates cardiac function after myocardial infarction. J Thorac Cardiovasc Surg 2003;126:114-23.
130. Ellis S, Rieke V, Kohi M, et al. Clinical applications for magnetic resonance guided high intensity focused ultrasound (MRgHIFU): present and future. J Med Imaging Radiat Oncol 2013;57:391-9.
131. McGann CJ, Kholmovski EG, Oakes RS, et al. New magnetic resonance imaging-based method for defining the extent of left atrial wall injury after the ablation of atrial fibrillation. J Am Coll Cardiol 2008;52:1263-71.
132. Peters DC, Wylie JV, Hauser TH, et al. Detection of pulmonary vein and left atrial scar after catheter ablation with three-dimensional navigator-gated delayed enhancement mr imaging: Initial experience. Radiology 2007;243:690-5.
133. Reddy VY, Schmidt EJ, Holmvang G, et al. Arrhythmia recurrence after atrial fibrillation ablation: Can magnetic resonance imaging identify gaps in atrial ablation lines? J Cardiovasc Electrophysiol 2008;19:434-7.

Cite this article as: Saeed M, Van TA, Krug R, Hetts SW, Wilson MW. Cardiac MR imaging: current status and future direction. Cardiovasc Diagn Ther 2015;5(4):290-310. doi: 10.3978/j.issn.2223-3652.2015.06.07

© Cardiovascular Diagnosis and Therapy. All rights reserved.